Electronic Supplementary Material (ESI) for Journal of Materials Chemistry A.

Supporting Information

An Ultralow-Temperature Aqueous Zinc-ion Battery

Tianjiang Sun, Xuming Yuan, Ke Wang, Shibing Zheng, Jinqing Shi, Qiu Zhang, Wensheng Cai, Jing Liang, Zhanliang Tao*

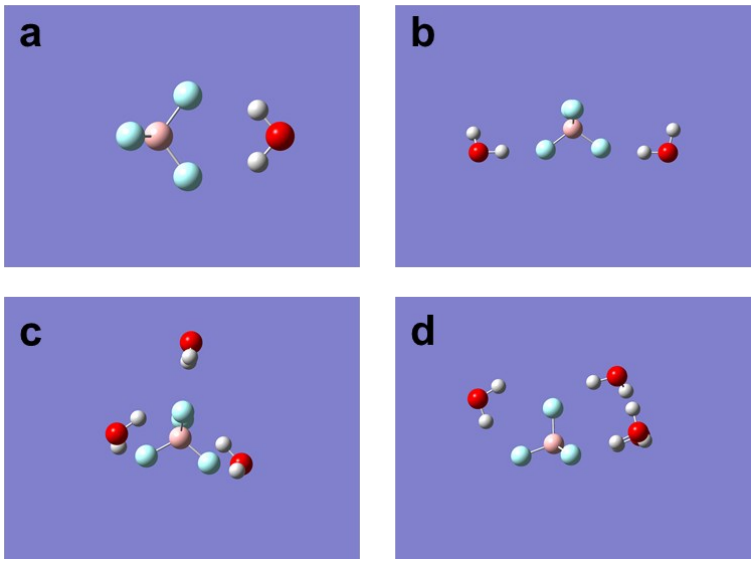

Figure S1. The structures optimization of one BF_4^- anion with one to four water molecules from DFT calculation. a) BF_4^--1 H_2O; b) BF_4^--2 H_2O; c) BF_4^--3 H_2O; d) BF_4^--4 H_2O.

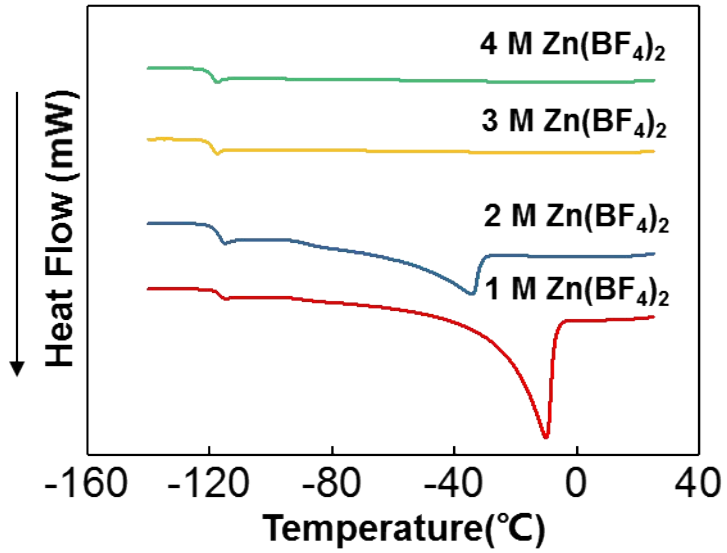

Figure S2. The DSC for different concentration of $Zn(BF_4)_2$ electrolyte (cooling).

From Figure S2, Different from traditional water, different concentrations (3, 4 M) of $Zn(BF_4)_2$ electrolytes undergo vitrification phase (amorphous phase) transition at low temperature. So that the DSC curves in Figure S2 shows no distinct valleys. The DSC curves of 1 M and 2 M $Zn(BF_4)_2$ electrolytes show two valleys, suggesting they undergo two solid phase transitions.

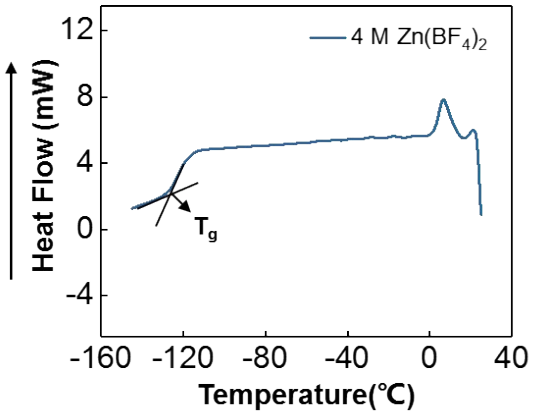

Figure S3. The DSC for 4 M $Zn(BF_4)_2$ electrolyte (heating).

From Figure S3, the glass transition temperature (T_g) is about -125 °C.

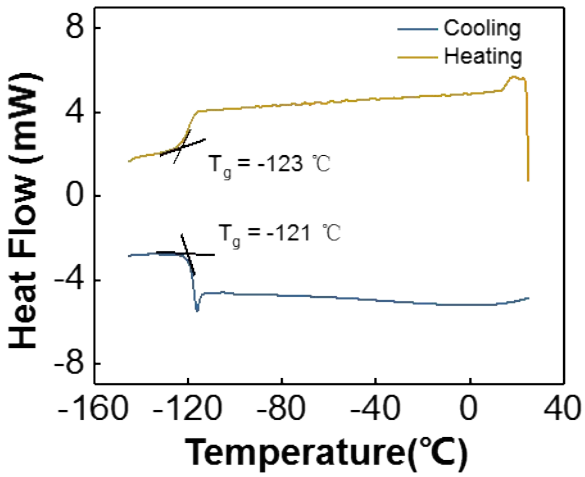

Figure S4. The DSC for 4 M $Zn(BF_4)_2$ electrolyte by adding Ketjen Black (KB).

Ding et al. reported that the some nucleating agent (for example, activated carbon, carbon black, and mesocarbon microbeads) can trigger the formation of a solid phase that is thermodynamically more stable when the electrolyte at low temperature.[1] In this work, KB was used as conductive agent. To measure the freezing point accurately, we studied the freezing process of 4 M $Zn(BF_4)_2$ electrolyte by adding KB (0. 5 mg mL^{-1}). From Figure S4, the T_g is about -121 °C, which is close with pure 4 M $Zn(BF_4)_2$ electrolyte.

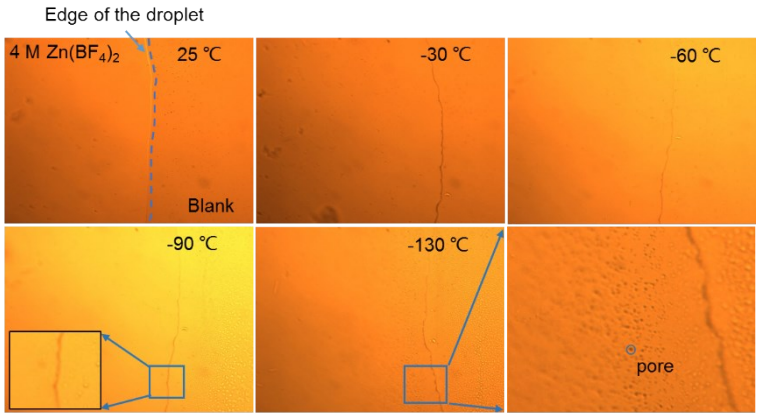

Figure S5. In situ non-polarizing microscope observation for 4 M $Zn(BF_4)_2$ electrolyte.

From Figure S5, we observed the morphology change of edge of the droplet at different temperature. The area on the left of the figure corresponds to 4 M $Zn(BF_4)_2$ electrolyte. It is clearly discover that the electrolyte has no change when temperature reduced to -90 °C. When temperature further drop to -130 °C, some pore appeared in the surface of electrolyte, indicating the 4 M $Zn(BF_4)_2$ electrolyte has transformed from liquid state to solid state. The gas in the electrolyte is expelled to form a pore when the electrolyte solidifies.

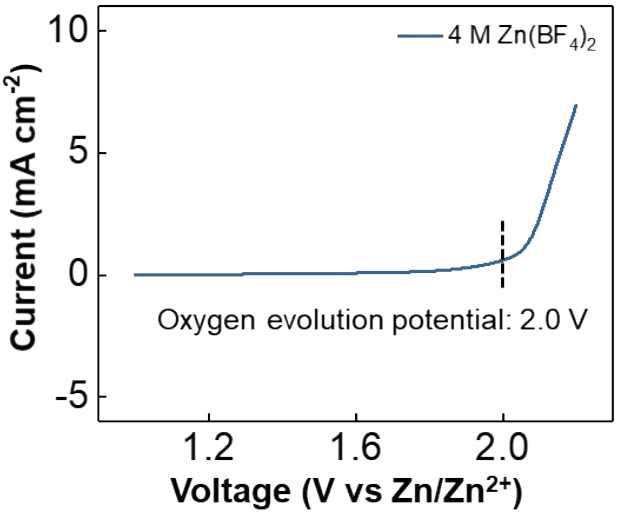

Figure S6. The oxidative stability of 4 M $Zn(BF_4)_2$ electrolyte.

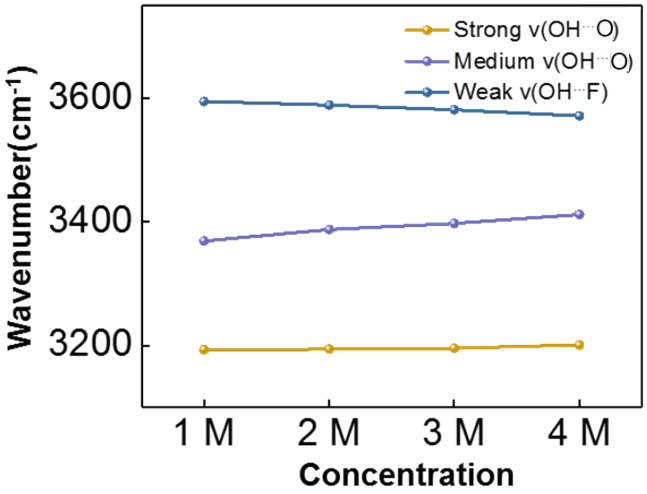

Figure S7. The peak shift of medium OH···O HBs and OH···F HBs.

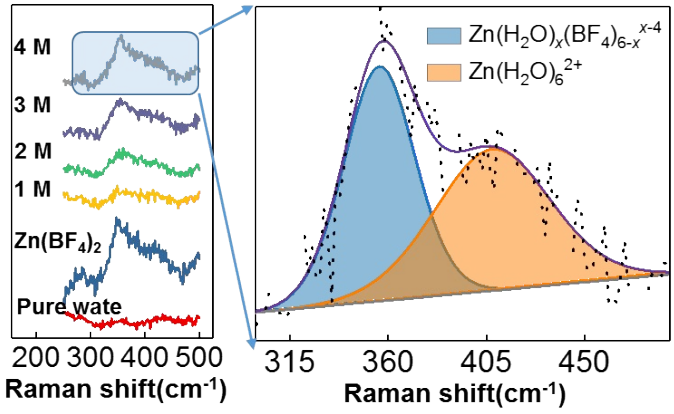

Figure S8. The Raman peak of solvation effect.

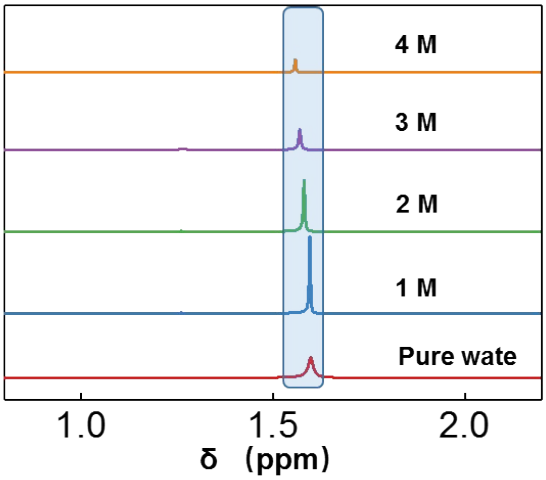

Figure S9. ^{1}H NMR spectrum of different electrolytes.

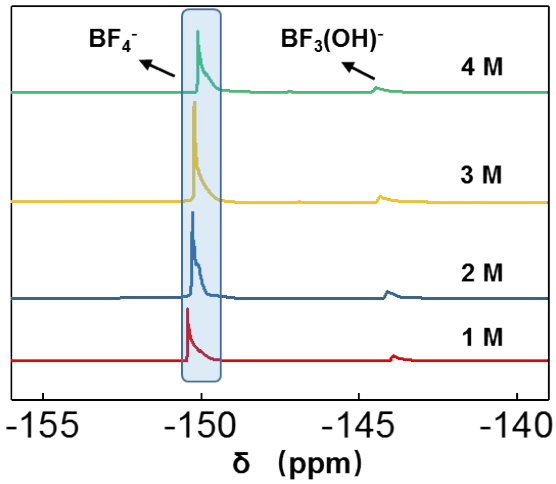

Figure S10. ^{19}F NMR spectrum of different electrolytes.

Form Figure S10, the strong resonance at -150.4 ppm is refer to BF_4^- anion. The peak has shift to high field, which imply the formation of hydrogen bond between BF_4^- anion and water molecules. Additionally, the very weak resonance at -144 ppm most likely represent $BF_3(OH)^-$ anion.[2] It is possible that it was formed during defluorination reaction of BF_4^- anion with water (in the first step: $BF_4^- + H_2O \leftrightarrow BF_3(OH)^- + HF$) on the silica surface.[3] Note that glass nuclear magnetic tube are used as containers, there are some floccules existed in electrolyte after resting long time, which may attribute to defluorination reaction. However, we find that the above defluorination reaction did not occur when the electrolyte is stored in a plastic tube.

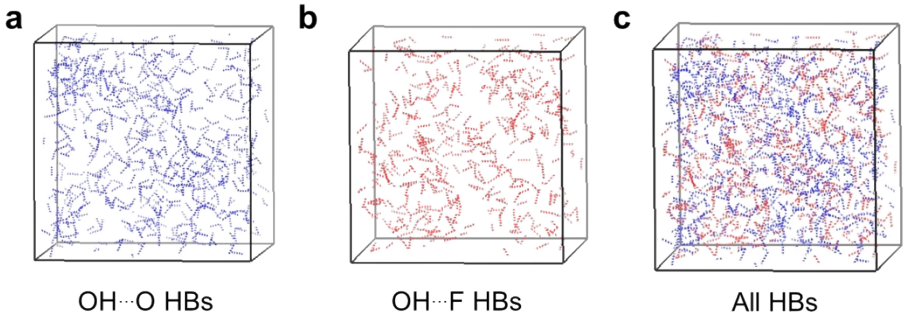

Figure S11. The distribution of different types HBs. a) OH···O HBs; b) OH···F HBs; c) All HBs.

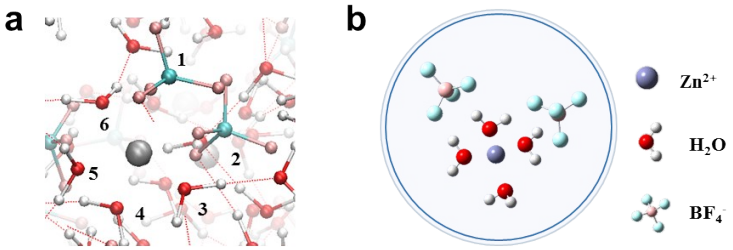

Figure S12. The solvation structure of $Zn(H_2O)_4(BF_4)_2$. a) The snapshot from MD simulation; b) The structures optimization of $Zn(H_2O)_4(BF_4)_2$ from DFT calculation.

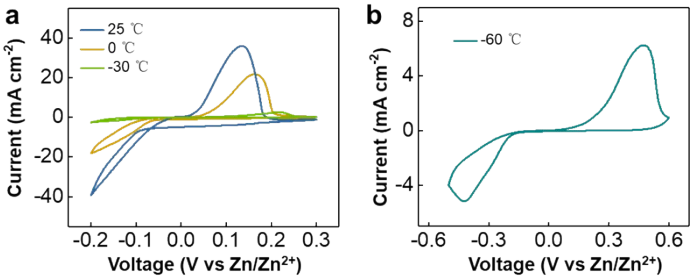

Figure S13. The CV curves of Zn//SS battery at different temperature. a) at 25, 0 and -30 °C; b) at -60 °C.

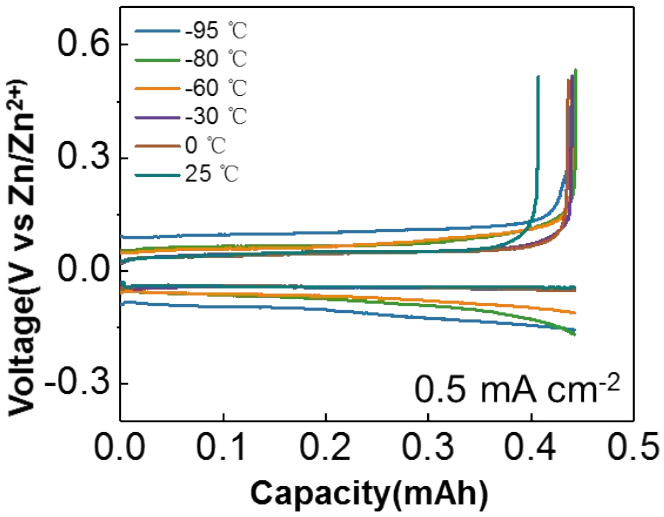

Figure S14. The charge-discharge curves of Zn//SS battery at different temperature.

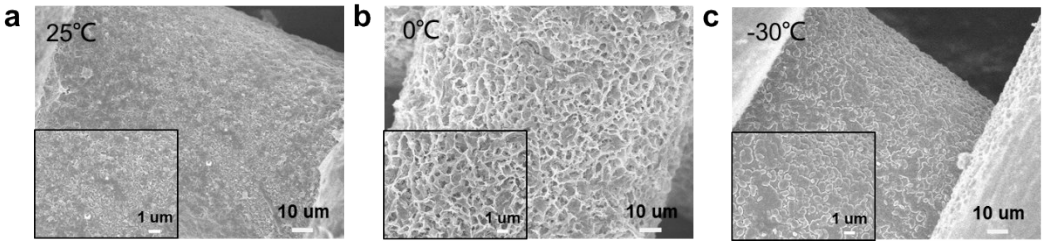

Figure S15. The depositional morphologies of Zn on SS at different temperature (Zn deposition amount is 5 mAh cm^{-2}). a) 25 °C; b) 0 °C; c) -30 °C.

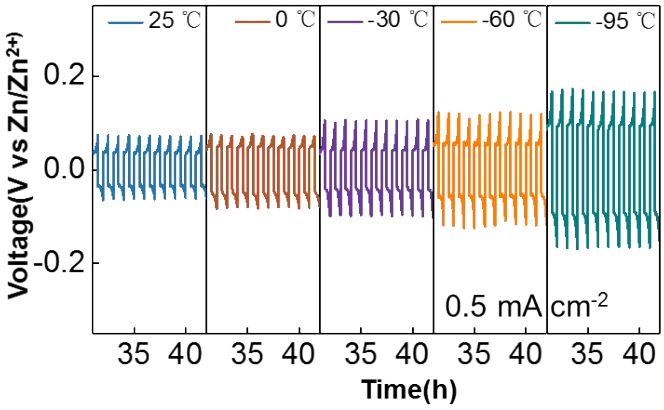

Figure S16. The voltage hysteresis of symmetric Zn//Zn battery at different temperature.

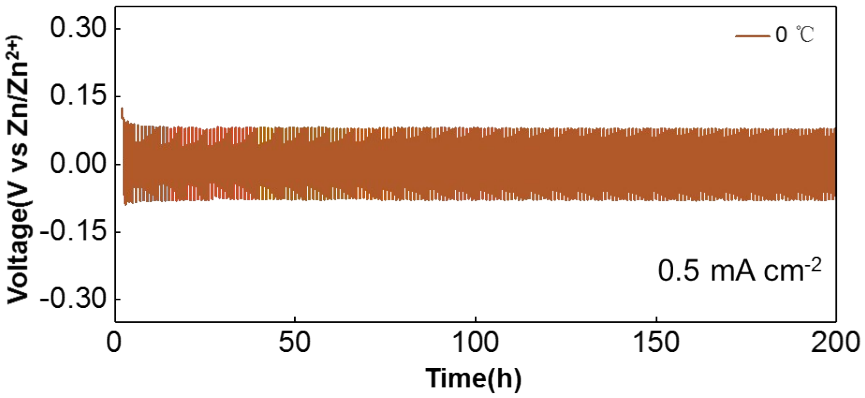

Figure S17. The cycling stability of symmetric Zn//Zn battery at 0 °C.

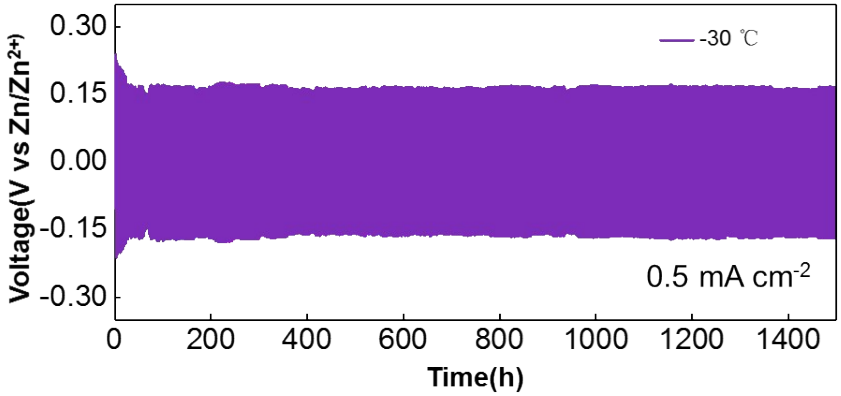

Figure S18. The cycling stability of symmetric Zn//Zn battery at -30 °C.

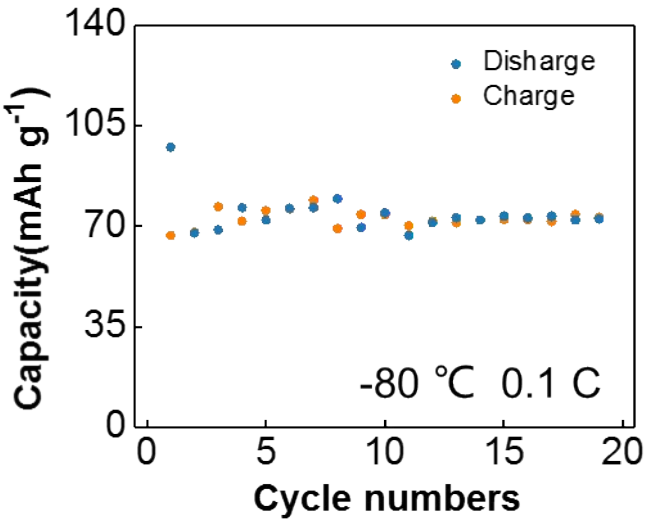

Figure S19. The cycling stability of Zn//TCBQ battery at -80 °C.

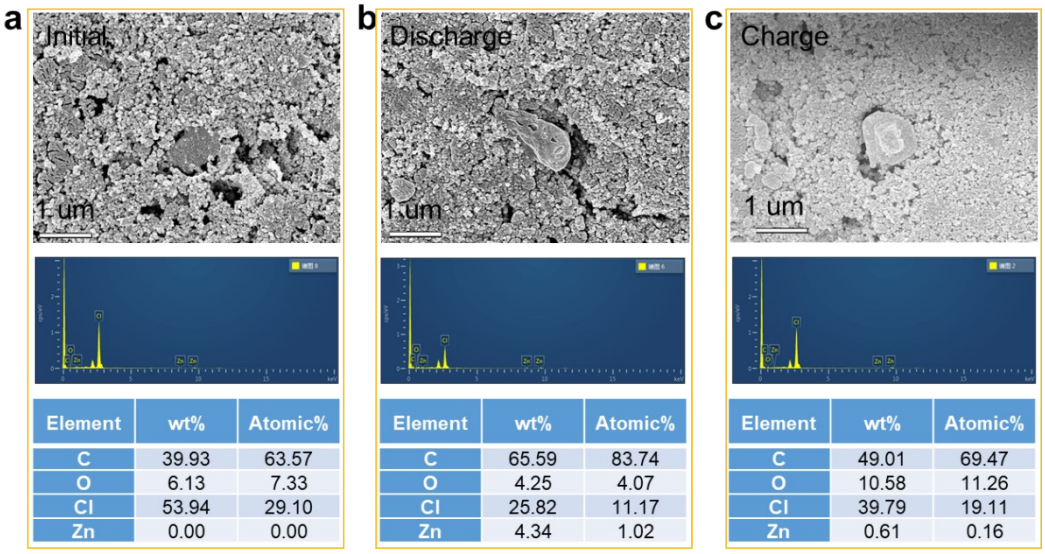

Element	wt%	Atomic%
C	39.93	63.57
O	6.13	7.33
Cl	53.94	29.10
Zn	0.00	0.00

Element	wt%	Atomic%
C	65.59	83.74
O	4.25	4.07
Cl	25.82	11.17
Zn	4.34	1.02

Element	wt%	Atomic%
C	49.01	69.47
O	10.58	11.26
Cl	39.79	19.11
Zn	0.61	0.16

Figure S20. The SEM and EDS of TCBQ at different state. a) Initial state; b) Discharge to 0.5 V; c) Charge to 1.5 V.

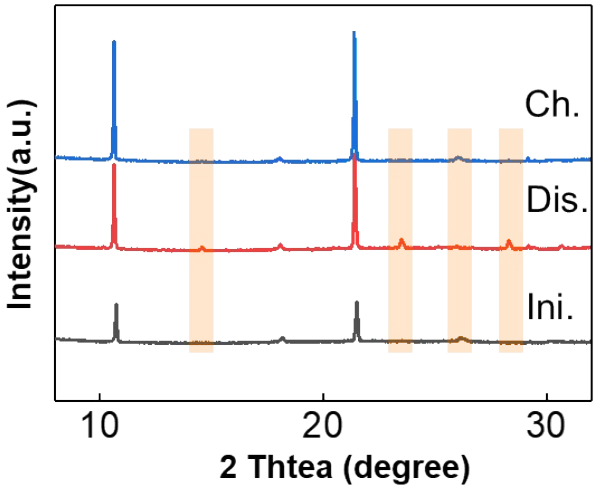

Figure S21. The ex-situ XRD of TCBQ (Ini.: Initial state; Dis.: Discharge state; Ch.: Charge state).

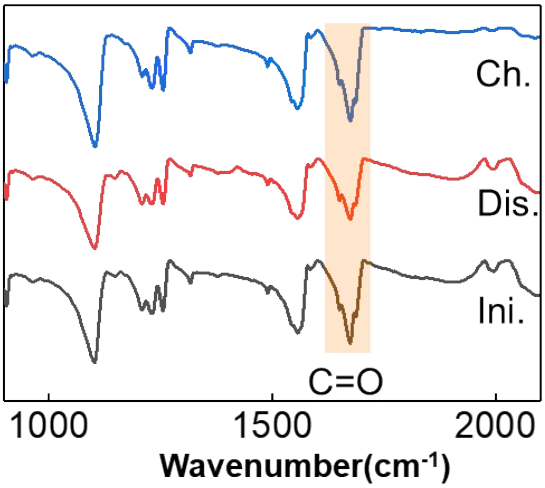

Figure S22. The ex-situ FTIR spectra of TCBQ

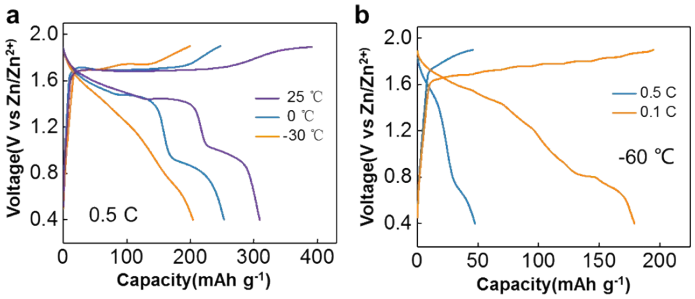

Figure S23. The charge-discharge curves of Zn//δ-MnO_2 battery at different temperature (1 C = 300 mAh g^{-1}). a) 25, 0 and -30 °C; b) -60 °C.

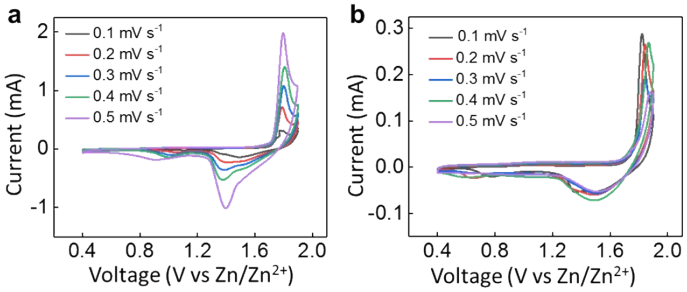

Figure S24. The CV curves of Zn//δ-MnO_2 battery at different temperature. a) 25; b) -30 °C.

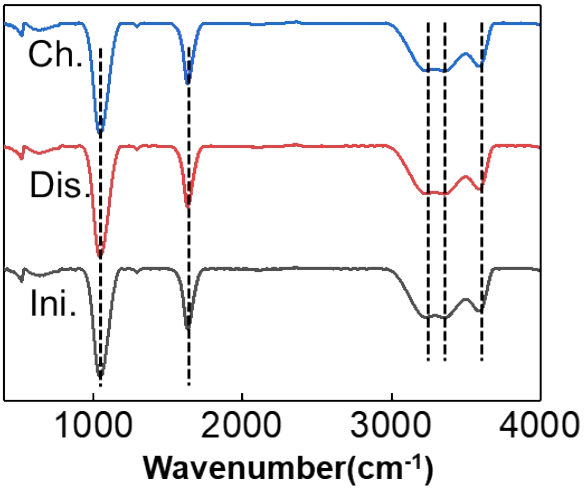

Figure S25. The ex-situ FTIR spectra of 4 M $Zn(BF_4)_2$ electrolyte.

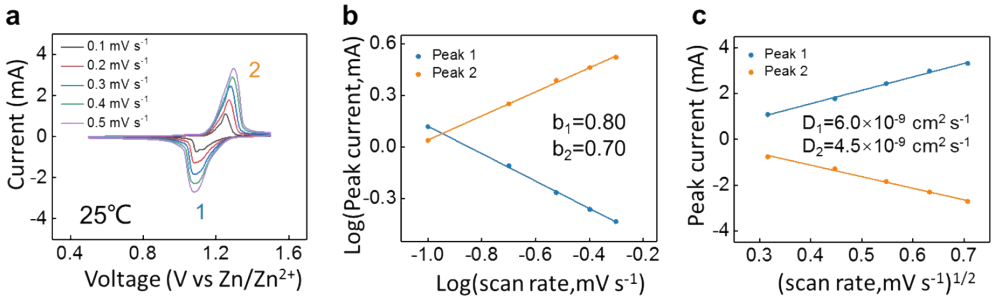

Figure S26. The kinetics calculation of Zn//TCBQ battery at 25 °C. a) The CV curves at different scan rates; b) The calculated b values; c) The calculated D values.

From Figure S26, The voltammetry response of Zn//TCBQ at various sweep rates can be summarized according to Eq.1[4]

$$i = av^b \quad (1)$$

where *a* and *b* are two adjustable parameters, *i* refers to the peak current (mA) and *v* corresponds to sweep rate (mV s^{-1}). The value of *b* shows the mechanism of charge storage. When the value of *b* is 0.5, it suggests the redox reaction is limited by semi-infinite diffusion, which is common in the conventional rechargeable batteries. When the value of *b* = 1, is suggests the mechanism is a capacitive behavior, where the rate performance is excellent.

The diffusion coefficient obeys the Equation:[5]

$$i_p = \left(2.69 \times 10^5\right) n^{3/2} \mathrm{A} \mathrm{D}^{1/2} v^{1/2} \mathrm{C}_{\circ} \quad (2)$$

i_p: Peak current; *n*: Transfer electron number; A: Area of electrode; D: Diffusion coefficients; *v*: scan rates; $C_{\circ}$: Concentration of ion.

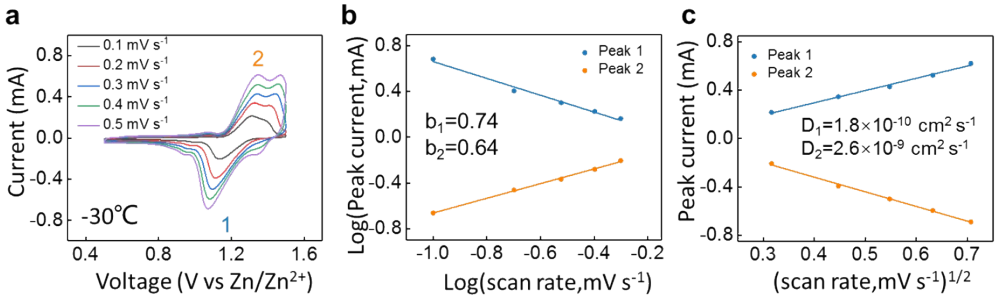

Figure S27. The kinetics calculation of Zn//TCBQ battery at -30 °C. a) The CV curves at different scan rates; b) The calculated b values; c) The calculated D values.

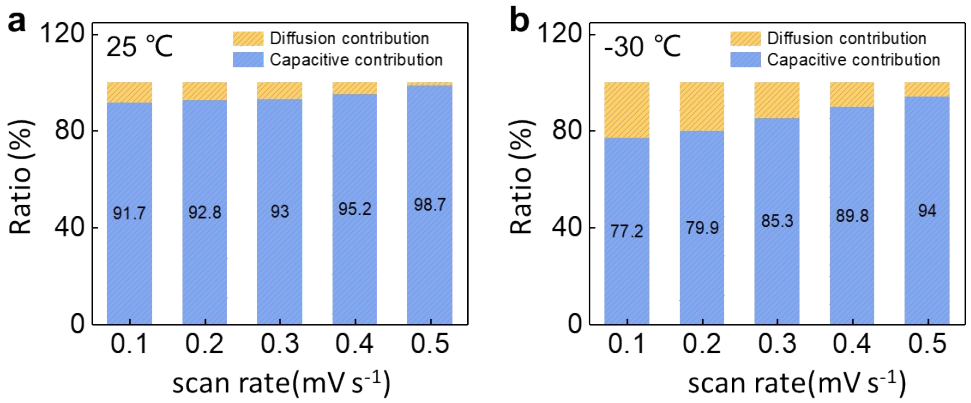

Figure S28. The capacitive contribution of Zn//TCBQ battery at different temperature. a) at 25 °C; b) at -30 °C.

From Figure S28, the capacitive contribution can be calculated through the following equation:[6]

$$i = k_1 v + k_2 v^{1/2} \quad (3)$$

$$\frac{i}{v^{1/2}} = k_1 v^{1/2} + k_2 \quad (4)$$

where $k_1 v$ refers to the capacitive contributions and $k_2 v^{1/2}$ corresponds to diffusion-controlled contributions.

Table S1. The single point energy from DFT calculations.

Molecules	Single point energy (Hartree)
H_2O	-76.209769
BF_4^-	-423.779304

Table S2. Comparison of binding energy for BF_4^- with different water molecules from DFT calculations.

Molecules	BSSE corrected energy (Hartree)	Interaction energy (kJ mol^{-1})
H_2O- H_2O	-152.427282	-20.33
BF_4^--1 H_2O	-499.788265	-50.04
BF_4^--2 H_2O	-576.009820	-80.99
BF_4^--3 H_2O	-652.239389	-134.27
BF_4^--4 H_2O	-728.470950	-190.19

Table S3. Comparison of electrochemical performance about reported low-temperature aqueous batteries (include Na^+, Zn^{2+} and H^+) with this work.

System	**Electrolyte**	**Freezing point (°C)**	**Discharge specific capacity/Current density /Temperature (mAh g^{-1}/mA g^{-1}/°C)**	**Energy density (Wh kg^{-1})**	**Ref.**
$NaTi_2(PO_4)_3$@C// Activated carbon	2 M $NaClO_4$+DMSO (molar fraction of 0.3)	-130	68/66.5/-50	73.2	[7]
Zn//polyaniline	7.5 M $ZnCl_2$	-114	50.6/10/-90	48.1	[8]
Zn//Activated carbon	2 M $ZnSO_4$+ethylene glycol (40% volume ratio)	-29	60/100/-20	36	[9]
$Cu^{II}[Fe^{III}(CN)_6]_{2/3}\cdot 4H_2O$ //MoO_3	9.5 M H_3PO_4	-85	28/25/-78	24	[10]
$NaTi_2(PO_4)_3$@C// NiOH	2 M NaClO4	/	78/1330/-20	40.1	[11]
$Na_{0.44}MnO_2$//Phenazine	10 M NaOH	/	98/1200/-20	68.6	[12]
GF@MnO_2//MoO_3	2 M H_2SO_4 + 2 M $MnSO_4$	-40	171.8/100/-70	177.4	[13]
GF@MnO_2// pyrene-4,5,9,10-tetraone	2 M H_2SO_4 + 2 M $MnSO_4$	-40	110/0.4 mA cm^{-2}/-70	99	[14]
Zn//TCBQ	**4 M $Zn(BF_4)_2$**	**-122.3**	**63.5/25/-95**	**76.2**	**This work**

Reference

1. K. X. S. P. Ding, S. S. Zhang, T. R. Jow. K. Amine, and G. L. Henriksen, *J. Electrochem. Soc.*, 1999, **146**, 3974-3980.
2. R. A. Oliveira, R. O. Silva, G. A. Molander and P. H. Menezes, *Magn. Reson. Chem.*, 2009, **47**, 873-878.
3. K. K. a. D. M. Grant, *J. Phy. Chem.*, 1964, **68**, 3208-3213.
4. T. Sun, C. Liu, X. Xu, Q. Nian, S. Zheng, X. Hou, J. Liang and Z. Tao, *J. Mater. Chem. A*, 2020, **8**, 21983-21987.
5. T. Sun, Q. Nian, S. Zheng, J. Shi and Z. Tao, *Small*, 2020, **16**, 2000597.
6. T. Sun, Q. Nian, S. Zheng, X. Yuan and Z. Tao, *J. Power Sources*, 2020, **478**, 228758.
7. Q. Nian, J. Wang, S. Liu, T. Sun, S. Zheng, Y. Zhang, Z. Tao and J. Chen, *Angew. Chem. Int. Ed.*, 2019, **58**, 16994-16999.
8. Q. Zhang, Y. Ma, Y. Lu, L. Li, F. Wan, K. Zhang and J. Chen, *Na.t Commun.*, 2020, **11**, 4463.
9. N. Chang, T. Li, R. Li, S. Wang, Y. Yin, H. Zhang and X. Li, *Energy Environ. Sci.*, 2020, **13**, 3527-3535.
10. H. Jiang, W. Shin, L. Ma, J. J. Hong, Z. Wei, Y. Liu, S. Zhang, X. Wu, Y. Xu, Q. Guo, M. A. Subramanian, W. F. Stickle, T. Wu, J. Lu and X. Ji, *Adv. Energy Mater.*, 2020, **10**, 2000968.
11. Q. Nian, S. Liu, J. Liu, Q. Zhang, J. Shi, C. Liu, R. Wang, Z. Tao and J. Chen, *ACS Appl. Energy Mater.*, 2019, **2**, 4370-4378.
12. T. Sun, C. Liu, J. Wang, Q. Nian, Y. Feng, Y. Zhang, Z. Tao and J. Chen, *Nano Res.*, 2020, **13**, 676-683.
13. L. Yan, J. Huang, Z. Guo, X. Dong, Z. Wang and Y. Wang, *ACS Energy Lett.*, 2020, **5**, 685-691.
14. Z. Guo, J. Huang, X. Dong, Y. Xia, L. Yan, Z. Wang and Y. Wang, *Nat. Commun.*, 2020, **11**, 959.